Applied Physics Letters

Spiral high-speed scanning tunneling microscopy: Tracking atomic diffusion on the millisecond timescale

Cite as: Appl. Phys. Lett. **119**, 251601 (2021); https://doi.org/10.1063/5.0071340
Submitted: 14 September 2021 • Accepted: 05 November 2021 • Published Online: 21 December 2021

L. Gura, Z. Yang, M. Brinker, et al.

Applied Physics Letters ARTICLE scitation.org/journal/apl

Spiral high-speed scanning tunneling microscopy: Tracking atomic diffusion on the millisecond timescale

Cite as: Appl. Phys. Lett. **119**, 251601 (2021); doi: 10.1063/5.0071340
Submitted: 14 September 2021 · Accepted: 5 November 2021 ·
Published Online: 21 December 2021

L. Gura, Z. Yang, M. Brinker, F. Kalaß, W. Kirstaedter, P. Marschalik, H. Junkes, M. Heyde,[a] and H.-J. Freund

AFFILIATIONS

Fritz-Haber-Institut der Max-Planck-Gesellschaft, Faradayweg 4-6, 14195 Berlin, Germany

[a]Author to whom correspondence should be addressed: heyde@fhi-berlin.mpg.de

ABSTRACT

Scanning tunneling microscopy (STM) is one of the most prominent techniques to resolve atomic structures of flat surfaces and thin films. With the scope to answer fundamental questions in physics and chemistry, it was used to elucidate numerous sample systems at the atomic scale. However, dynamic sample systems are difficult to resolve with STM due to the long acquisition times of typically more than 100 s per image. Slow electronic feedback loops, slow data acquisition, and the conventional raster scan limit the scan speed. Raster scans introduce mechanical noise to the image and acquire data discontinuously. Due to the backward and upward scan or the flyback movement of the tip, image acquisition times are doubled or even quadrupled. By applying the quasi-constant height mode and by using a combination of high-speed electronics for data acquisition and innovative spiral scan patterns, we could increase the frame rate in STM significantly. In the present study, we illustrate the implementation of spiral scan geometries and focus on the scanner input signal and the image visualization. Constant linear and constant angular velocity spirals were tested on the Ru(0001) surface to resolve chemisorbed atomic oxygen. The spatial resolution of the spiral scans is comparable to slow raster scans, while the imaging time was reduced from ∼100 s to ∼8 ms. Within 8 ms, oxygen diffusion processes were atomically resolved.

Scanning tunneling microscopy (STM) has proven to be a powerful tool in surface science. While the spatial resolution is extraordinary good, the time resolution is very low. Typical image acquisition times in conventional STM are on the order of 100 s.

A significant increase in the frame rate opens new possibilities to study dynamic systems.[1,2] Faster STMs would lead to higher prominence in academia and industry across different disciplines, such as life- and materials science.[3,4] Limiting factors and challenges for video-rate and high-speed STMs are discussed in the literature.[3,5] The image rate is mainly limited by three factors: (1) The electronic feedback to control the tunneling current is slow. (2) The data acquisition is too slow in conventional hardware and software. (3) The conventional raster scan geometry is inefficient and introduces mechanical noise to the scanner. The noise that couples to the scanner is further determined by the mechanical properties of the STM scanner unit.[6–8]

Some approaches exist to increase the frame rate by using special pre-amplifiers,[9–15] benefiting from the mechanical properties of the STM scanner,[16–18] or by applying slightly varied scan geometries. While unconventional scan geometries have already been explored in other scanning microscopy techniques, such as atomic force microscopy (AFM) and scanning transmission electron microscopy (STEM), STM still sticks to the conventional raster scan.

One drawback of the raster scan is the discontinuous data acquisition. Due to the backward scan or the flyback movement of the tip, the scan area is imaged four times within one measurement. The image contrast can vary significantly due to the rapidly changing scan direction. In addition, these rapid changes in the tip propagation direction and the tip velocity cause mechanical resonances in the system, which in turn distort the image.

Although variations from the triangular shaped raster scan in STM were performed by reducing the time-of-walk (TOW)[2] or by using sine waves as input signals for the fast scan direction,[19] these changes are minor compared to other scanning techniques, where Lissajous, cycloid, and spiral trajectories have been tested.[20–28]

So far, unconventional scan patterns have not been employed to increase the frame rate in STM. This is surprising considering that the advantages of unconventional scans in scanning probe micoscopy (SPM) are widely discussed in the literature.[20,23,27,29–34]

To shift the paradigm from the inefficient raster scan to innovative scan patterns, we show a pathway toward higher frame rates with atomic resolution. In this study, we apply the spiral scan pattern to STM, which implies important adjustments of the input signal generation. We present high-speed STM images acquired with spiral geometries. The image resolution is comparable to conventional slow scans. With the increased frame rate at high spatial resolution, this innovation can broaden the field of scientific applications in many disciplines, in both academia and industry.

To test different spiral geometries and to compare them with slow raster scan images, we imaged the hexagonal structure of the 3O (2×2) adlayer on Ru(0001). The system is well studied by STM and is important for catalytic reactions and for supported thin films.[35] In addition, we measured the dynamics of single oxygen atoms on the oxygen covered Ru(0001) surface in analogy to Wintterlin *et al.*[19]

The sample preparation and measurements were performed in ultrahigh vacuum (UHV) at a base pressure in the range of 10^{-9} mbar. STM images are acquired at room temperature with a custom designed and home built STM with a PtIr tip. The microscope design is similar to the Pan-STM[36] and exhibits low thermal drift characteristics due to its compact, rigid, and highly symmetric design. The piezoelectric scanner exhibits a high resonance frequency of above 1 MHz.

The scanner can be driven in the conventional slow raster scan mode, for which commercial hardware is used. For the high-speed spiral scan, a Versa Module Eurocard-bus (VMEbus) system running Experimental Physics and Industrial Control System (EPICS) on Real-Time Executive for Multiprocessor Systems (RTEMS)[37] is used with a field programmable gate array (FPGA) of a maximum sampling rate of 250 MHz. The arbitrary waveform generator V375 from Highland Technology generates the input voltage signal for the tube piezo. The 14 bit digitizer SIS3316 from Struck collects the data and writes data chunks to a process variable (PV) that is provided within the EPICS framework.

To store the data, we use the pvapy python interface for EPICS,[38] which subscribes to the PV. In python, we create a producer thread to collect the frames in a queue on a local machine. A consumer thread stores the frames as hierarchical data format version 5 (HDF5) files. In parallel, another independent thread, which can run on a different machine, subscribes to the PV and collects frames. After basic processing of the data, live images of the spiral scan are provided within the EPICS framework. The resulting live video of the scan is displayed in a customized desktop application, which uses the Phoebus framework.[39] In the Phoebus desktop application, control tools for the spiral scan are implemented. This enables the live observation of scan results and the controlled selection and changing of the scan area for high-speed scans.

To create the spiral scan voltage input signals for the scanner, we developed a customizable signal generation that is realized via the arbitrary waveform generator. Further details of the scanner design, software implementation, and data acquisition are described in Ref. 40.

As reference for the image resolution, the 3O (2×2) layer on Ru(0001) is scanned with commercial electronic hardware and the conventional raster scan pattern. The resulting STM image is shown in Fig. 1(a). Oxygen atoms appear as protrusions and form the clearly resolved hexagonal structure. Different forms of raster scans exist, all exhibiting sharp points of inversion in the voltage input signal and the piezo-movement. For illustration, the line-by-line motion is schematically shown in Fig. 1(b). While the data sampling points are easily

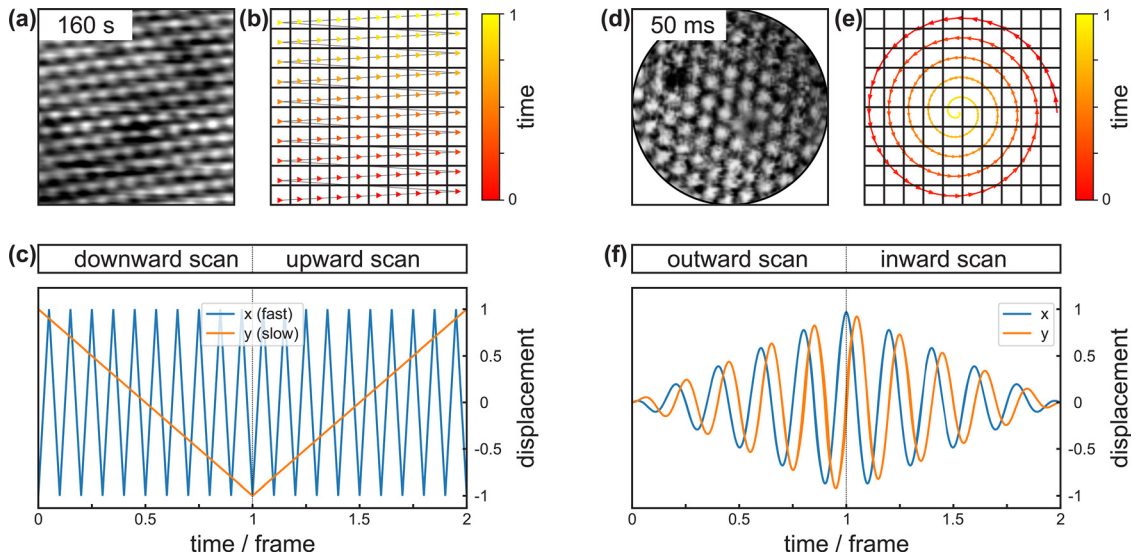

FIG. 1. Comparison of conventional raster and spiral scan STM. (a)–(c) Raster and (d)–(f) spiral geometry in STM. (a) and (d) Atomically resolved STM images of the 3O(2×2) structure on Ru(0001) ($V_S = 1$ V, $I_T = 1$ nA, 5×5 nm^2). (b) and (e) Schematic illustration of the raster and the spiral scan. The triangles represent data sampling points, indicate the scan direction, and are color coded as shown on the right inset. Two-dimensional grids are overlaid, representing the 2D array of image pixels. (c) and (f) Lateral displacement in x and y of the STM tip as a function of time in the raster and the spiral scan. For the raster geometry in (c), the fast and the slow scan direction are plotted for the forward and backward scans for both, downward and upward scan. For the spiral geometry in (f), the signal for outward and inward scan is smoothly connected without changes in the slope nor abrupt changes in the displacement.

mapped on a 2D grid to create the image, it becomes obvious that the data information is discontinuous due to the backward motion of the STM tip after each line. The abrupt changes in the scan direction are shown in Fig. 1(c). These sharp points of inversion introduce mechanical resonances to the system, which then distort the STM image. This effect is severe at high tip velocities. Not only the tip velocity limits the frame rate but also the fact that the tip scans the surface four times (up, down, forward, backward) per measurement cycle.

To scan with higher tip velocities and to reduce the time for one measurement cycle, the input signal must be smooth and the real space must be scanned efficiently. Lissajous, cycloid trajectories, and spiral geometries satisfy the requirement of smooth voltage input signals that transform to smooth lateral displacements of the tip. Main advantages of spirals are the continuous scan direction and the very efficient scan of the real space.

Spirals are subject in many areas of scientific research and are widespread in nature. Different mathematical expressions exist for spiral geometries. In the present study, we will stick to Cartesian coordinates because they directly relate to the voltage input signal and the lateral displacement of the scanner. Figure 1(d) shows the same oxygen covered Ru(0001) surface as Fig. 1(a) scanned with a spiral pattern. As in the slow raster scan, the oxygen atoms appear as protrusions and the hexagonal structure of the adlayer is clearly resolved. The image resolution is comparable to the slow raster scan image, while the acquisition time of 50 ms is more than 3000 times lower than for the conventional scan.

The high frame rate was achieved thanks to the spiral geometry schematically shown in Fig. 1(e). The data acquisition is continuous, and the data points can be mapped on the shown 2D grid by averaging the intensities per grid point. Details of the image reconstruction are explained later.

The input signals for the x- and y-direction are smooth, as shown in Fig. 1(f). To avoid image distortions, we pursued the main idea to avoid abrupt changes in the scan speed and the tip displacement. Therefore, the outward and inward scans are combined smoothly.

The spiral scan is widely adjustable and customizable with parameters a and b as given in the following equations:

$$x = t^a \cdot \cos(\omega \cdot t^b), \tag{1}$$

$$y = t^a \cdot \sin(\omega \cdot t^b), \tag{2}$$

x and y are the spatial coordinates as drawn in Fig. 1(f). t resembles the time. The frequency ω adjusts the line density in a spiral within a given time. The line density can also be expressed in terms of the distance between two neighbored lines (pitch size) or the number of rotations of the STM within one frame. If the number of rotations is fixed, two parameters tune the spiral geometry and tip velocity. a changes the amplitude of the scan input signal over time and, therefore, allows to drive different spiral geometries, such as Archimedean or Fermat spirals.[26] With constant sampling frequencies, the acquired data points are equidistant in time. b adjusts the data point density in real space along the tip trajectory and changes the tip velocity from constant linear velocity (CLV) to constant angular velocity (CAV), for instance. CLV and CAV scans are compared later in terms of image resolution.

First, we focus on the implementation of the spiral signal to STM. The implementation is independent of the parameters ω, a, and b. Therefore, for simplicity, the Archimedean spiral at CAV is used as example. Most importantly, the spiral signal implementation is independent of the STM scanner design. The signal is generally applicable and only small adjustments are necessary.[41–43] Our setup, for instance, uses a four-segmented piezoelectric tube to perform the scanning motion.[44]

To avoid the limiting electronic feedback loop, we scan in quasi-constant height mode. In this mode, a slow feedback loop that does not interfere with the spiral scan compensates thermal drifts. As in constant height mode, the tilting between the plane of the lateral movement of the STM tip and the scanned surface must be corrected in x and y directions. Figure 2(a) sketches the tilt angle α in the x-direction. The z input signal, which changes the tip-sample distance, is used to correct for the tilting between sample surface and scanner. z depends on the tilt angles in x and y directions (α and β) and is a linear combination of the input signals for the lateral tip displacement in x and y, as given in the following equation:

$$z = \tan(\alpha) \cdot x + \tan(\beta) \cdot y. \tag{3}$$

Figure 2(b) shows the tip displacement in x, y, and z for the outward scan of the Archimedean spiral at CAV. Due to the Archimedean geometry, the amplitudes of the sine waves increase linearly with time. x and y are phase shifted by 90°. z is exemplarily shown for the case that the tilt angles α and β are the same. The displacement

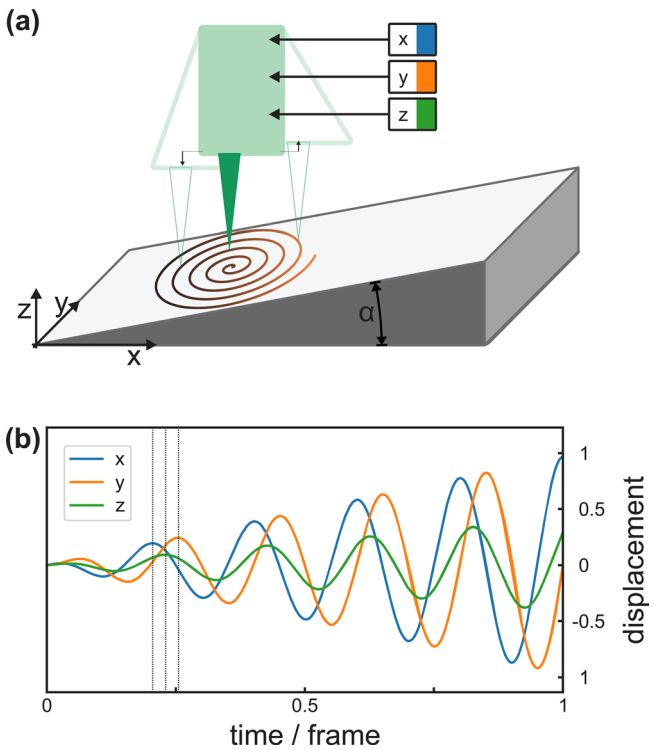

FIG. 2. Tilt correction for the spiral scan geometry. (a) Scheme of the tilt angle α between the plane of lateral movement of the STM tip and the sample surface. The three color coded input signals x, y, and z are connected to the STM scanner and produce the height corrected spiral scan geometry. (b) Tip displacement in x, y, and z over time. The three dotted lines illustrate the phase shift of x, y, and z.

of z is scaled arbitrary, because it depends on the proportion of lateral and vertical displacement of the STM scanner unit.

The input signal is completely customizable in terms of the scan geometry and the tip velocity. Figure 3 shows two spiral scans on the same 3O(2 × 2) covered Ru(0001) surface. In Fig. 3(a), the tip scans with constant linear velocity. The sampling points (triangles) are equidistant along the scan trajectory and are homogeneously distributed. The tip moves faster in the center and slower at the rim. In Fig. 3(b), the tip scans with constant angular velocity. In contrast to the CLV scan, the sampling points are not equidistant along the scan trajectory. This is due to the fact that the sampling frequency is constant and that the tip spends the same time for the inner and the outer rotations. In terms of sampling point distribution, the CLV scan is favorable. However, Figs. 3(c) and 3(d) show that the image contrast in STM images varies significantly between CLV and CAV scans. While the CAV scan shows clearly resolved atomic sites, especially in the center of the image, the CLV scan shows uniform but in general lower image contrast. Therefore, the CAV scan seems to be preferable for spiral STM measurements. Further parameter studies are the scope of future studies.

As mentioned above, the spiral data points do not represent 2D grid points. Therefore, a display method must be developed to visualize the point cloud. In the following, we use the CAV scan from Fig. 3(d) to demonstrate different image reconstruction methods. To visualize and to analyze spiral scan images, we are developing a purely Python-based program, which is freely accessible.[45] Besides numerous 1D signal filters and 2D image filters, we implemented different image reconstruction methods.

Figure 4 shows three different methods to display the non-grid data as a two-dimensional image. Computationally most feasible is the 2D histogram. The equidistant 2D grid bins the point cloud, and the average intensity values are assigned to the corresponding bins. The smallest unit of the grid is the area of 1 bin × 1 bin. Therefore, this area can be represented as one pixel in a 2D raster image. The aforementioned live display of the spiral scan needs such a fast routine. As example, we provide a real time video in the supplementary material, which shows consecutive 2D histograms reconstructed from unfiltered data. The 2D histogram images exhibit atomic resolution and have few empty pixels for small image dimensions up to $\frac{\omega}{2}$ pixels.

However, for larger image sizes, the pixels without data points increase. Figure 4(a) gives an example of such a 2D histogram with 300 bins × 300 bins that exhibits many "empty" pixels. In the zoomed

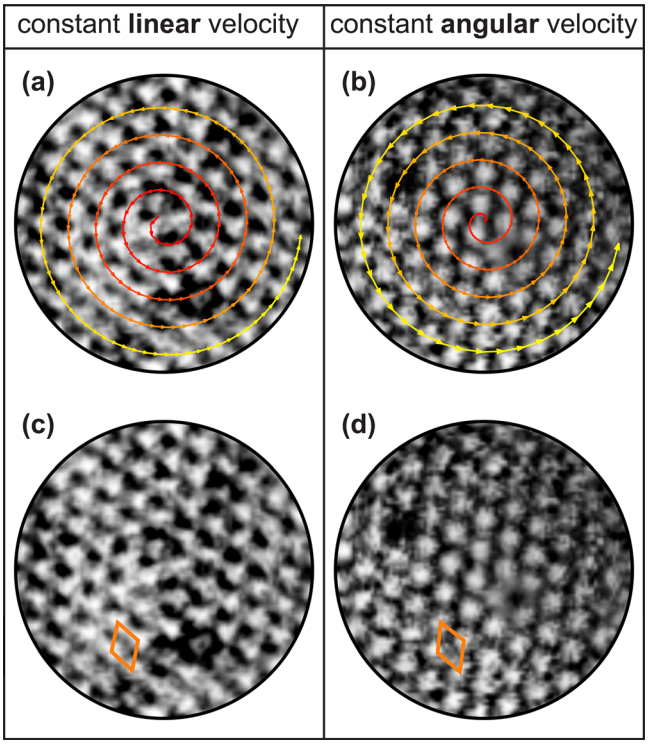

FIG. 3. Constant linear and constant angular velocity in spiral STM. The figure reads like a table. (a) and (b) Spiral STM images with overlaid schematical tip trajectories for constant linear and constant angular tip velocities, respectively. For visualization, triangles represent data sampling points, in analogy to Fig. 1. (c) and (d) The respective STM images of the 3O(2 × 2) structure on Ru(0001) with the unit cell drawn in orange. Scan parameters for all images: $V_S = 1$ V, $I_T = 1$ nA, scan diameter = 5 nm, acquisition time per image: 8.3 ms. Time stamps are given in the images.

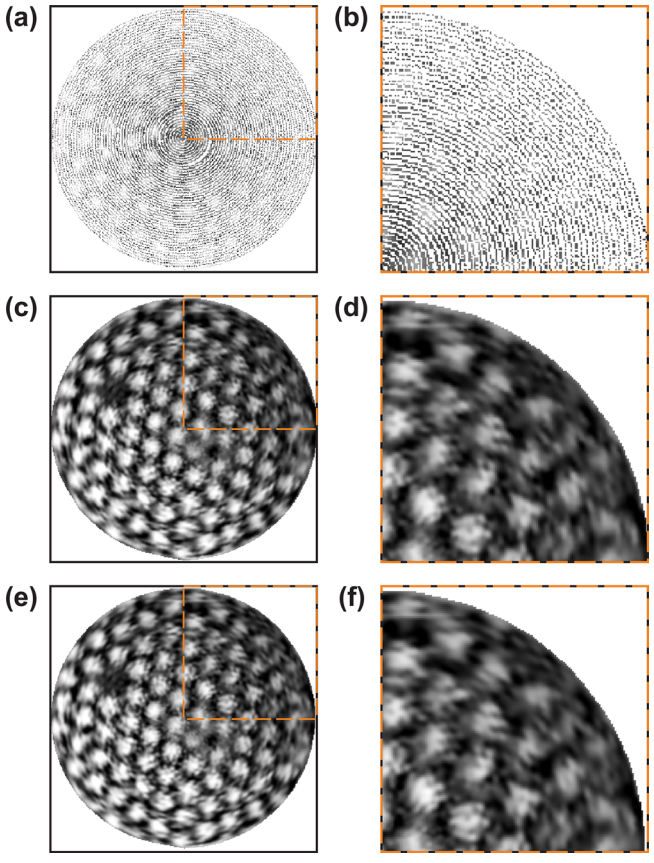

FIG. 4. Image reconstruction of spiral STM scans. The reconstruction is based on the same dataset as presented in Fig. 3(d). (a) 2D histogram with 300 bins × 300 bins and (b) zoomed section of (a). (c) STM image reconstructed on the basis of (a) with the inpaint algorithm and (d) zoomed section of (c). (e) Interpolated STM image from the acquired point cloud and (f) zoomed section of (e).

section in Fig. 4(b), the spiral trajectory is visible and the image contrast that shows atomic resolution is hardly detectable. Based on this 2D histogram, the image in Fig. 4(c) is reconstructed with the inpaint algorithm, which is implemented in the scikit-image python package.[46] The atoms are clearly resolved, and the image contrast is more pleasant for the human eye, compared to the 2D histogram. Even in the zoomed section in Fig. 4(d), the image contrast is very good. Figure 4(e) shows the interpolated point cloud that is mapped on an 300×300 pixels 2D raster image. For the interpolation, the scipy python package is used.[47] The image contrast is similar to the inpainted image. This becomes obvious comparing the zoomed sections in Figs. 4(d) and 4(f).

While the image contrast of inpainted and interpolated images is very pleasant for the human eye due to the increased pixel number, these image reconstructions are computational expensive. Therefore, they are most suitable for post-processing of high-speed scans.

To demonstrate the high-speed capability of spiral STM, we measured the dynamic system of chemisorbed atomic oxygen on Ru(0001). The acquired images in Fig. 5 are reconstructed with the inpaint algorithm. Each image was acquired in 8.3 ms, which corresponds to a frame rate of 120 Hz.

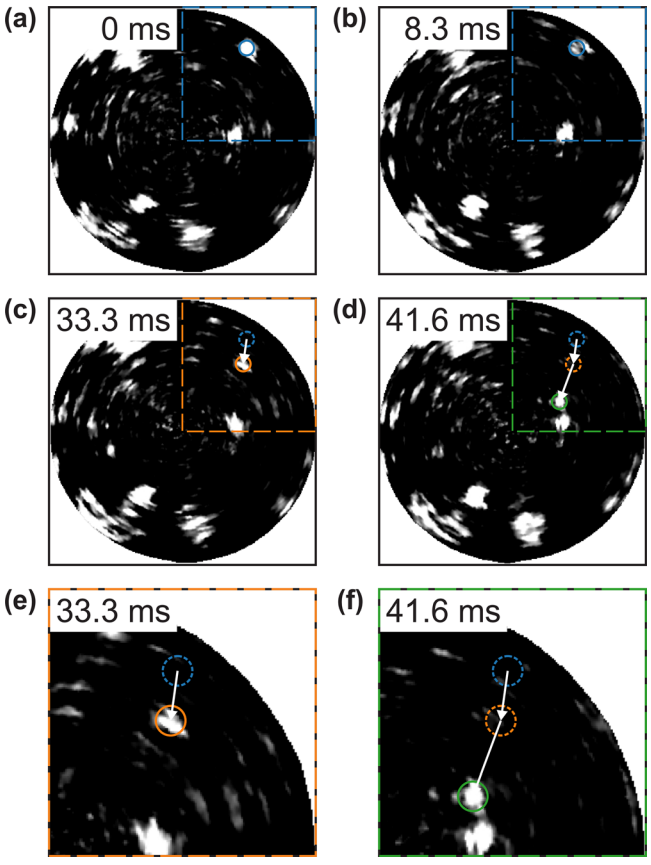

FIG. 5. Dynamics of single oxygen atoms on Ru(0001) captured with spiral STM. (a)–(d) High-speed spiral STM image with atomically resolved single oxygen atoms on Ru(0001). (e) and (f) Zoomed sections from (c) and (d), respectively. The oxygen atom positions are marked with color coded circles. Two hopping events are observed. Scan parameters for all images: $V_S = 0.9$ V, $I_T = 2$ nA, scan diameter = 5 nm, and acquisition time: 8.3 ms.

In the following discussion, we focus on the marked sections in the upper right corner of the spiral STM images. Two oxygen atoms are resolved in this section. From frame (a) to frame (b), the atoms stay at their positions. Then, the upper atom jumps to a lower position, as marked in Fig. 5(e). After another 8.3 ms, the atom jumps a longer distance, as visualized in Fig. 5(f).

Thanks to the spiral scan geometry, we were able to increase the frame rate of our STM to resolve these fast atomic dynamics. In our custom-developed visualization program, we implemented tools to track features over time and analyze their dynamics. These tools enable future investigations of diffusion processes and other dynamic processes, such as chemical reactions and structural changes.

The spiral scan modes that we tested, namely, CLV and CAV Archimedean scans, showed atomic resolution with similar contrast as the slow raster scan. In the presented case, the CAV spiral scan showed higher image contrast, especially in the center of the image. In future works, the influence of the spiral geometry, especially of the parameters a and b, will be investigated. The high-speed spiral scans resolved the dynamics of atomic oxygen on Ru(0001) with a time resolution that exceeds reported STM frame rates. Considering that these images are the first spiral STM images and that more parameter studies and innovations in terms of electronic hardware can push the limits further, we are confident that spiral STM opens up the possibility to resolve sub-millisecond dynamics.

We have shown that spiral scan patterns can be implemented in STM to increase its frame rate. The spiral geometry is applicable to any STM scanner design. We discussed image reconstruction methods based on acquired spiral STM data. To overcome the challenge of data visualization and analysis of non-raster images, we provide a freely accessible Python-based software for the analysis of data point clouds. We showed the capability of spiral STM to capture dynamics at the atomic scale in the millisecond range, and we are convinced that soon sub-millisecond dynamics are accessible with this setup. With this proof of principle, we hope to set the start for a paradigm shift in the STM community regarding the scan pattern design.

See the supplementary material that includes a high-speed spiral STM video. The video shows the Ru(0001) surface covered with atomic oxygen (coverage = 0.1). Every frame represents a 2D-histogram with 100×100 grid points of the unfiltered raw data. Using this display method, this video is an example of the live video that can be viewed by the user during the STM measurement, as mentioned in the main manuscript. For visualization, the intensity range of the frames is adjusted (equalization). The frame rate of the video is 30 Hz, i.e., every frame is acquired within 33.3 ms. The displayed real time at the bottom of the video is extracted from the real time operating system RTEMS. As implied by the displayed time, the provided video is extracted from a longer recorded sequence. The total length of the recorded sequence is 4 min.

This project has received funding from the European Research Council (ERC) under the European Unions Horizon 2020 Research and Innovation Program (Grant Agreement No. 669179). L.G. acknowledges support by the IMPRS for Elementary Processes in Physical Chemistry.

AUTHOR DECLARATIONS

Conflict of Interest

The authors have no conflicts to disclose.

DATA AVAILABILITY

The data that support the findings of this study are available from the corresponding author upon reasonable request.

REFERENCES

[1]O. Magnussen and M. Vogt, "Dynamics of individual atomic kinks during crystal dissolution," Phys. Rev. Lett. **85**, 357 (2000).

[2]O. Magnussen, W. Polewska, L. Zitzler, and R. Behm, "*In situ* video-STM studies of dynamic processes at electrochemical interfaces," Faraday Discuss. **121**, 43–52 (2002).

[3]G. Schitter and M. J. Rost, "Scanning probe microscopy at video-rate," Mater. Today **11**, 40–48 (2008).

[4]O. M. Magnussen, "Atomic-scale insights into electrode surface dynamics by high-speed scanning probe microscopy," Chem. Eur. J. **25**, 12865–12883 (2019).

[5]C. Y. Nakakura, V. M. Phanse, G. Zheng, G. Bannon, E. I. Altman, and K. P. Lee, "A high-speed variable-temperature ultrahigh vacuum scanning tunneling microscope," Rev. Sci. Instrum. **69**, 3251–3258 (1998).

[6]M. J. Rost, G. J. C. van Baarle, A. J. Katan, W. M. van Spengen, P. Schakel, W. A. van Loo, T. H. Oosterkamp, and J. W. M. Frenken, "Video-rate scanning probe control challenges: Setting the stage for a microscopy revolution," Asian J. Control **11**, 110–129 (2009).

[7]S. Behler, M. K. Rose, D. F. Ogletree, and M. Salmeron, "Method to characterize the vibrational response of a beetle type scanning tunneling microscope," Rev. Sci. Instrum. **68**, 124–128 (1997).

[8]B. J. Kenton, A. J. Fleming, and K. K. Leang, "Compact ultra-fast vertical nanopositioner for improving scanning probe microscope scan speed," Rev. Sci. Instrum. **82**, 123703 (2011).

[9]R. Curtis, T. Mitsui, and E. Ganz, "An ultrahigh vacuum high speed scanning tunneling microscope," Rev. Sci. Instrum. **68**, 2790–2796 (1997).

[10]M. J. Rost, L. Crama, P. Schakel, E. van Tol, G. B. E. M. van Velzen-Williams, C. F. Overgauw, H. Ter Horst, H. Dekker, B. Okhuijsen, M. Seynen, A. Vijftigschild, P. Han, A. J. Katan, K. Schoots, R. Schumm, W. van Loo, T. H. Oosterkamp, and J. W. M. Frenken, "Scanning probe microscopes go video rate and beyond," Rev. Sci. Instrum. **76**, 053710 (2005).

[11]F. Esch, C. Dri, A. Spessot, C. Africh, G. Cautero, D. Giuressi, R. Sergo, R. Tommasini, and G. Comelli, "The fast module: An add-on unit for driving commercial scanning probe microscopes at video rate and beyond," Rev. Sci. Instrum. **82**, 053702 (2011).

[12]K. M. Bastiaans, T. Benschop, D. Chatzopoulos, D. Cho, Q. Dong, Y. Jin, and M. P. Allan, "Amplifier for scanning tunneling microscopy at MHz frequencies," Rev. Sci. Instrum. **89**, 093709 (2018).

[13]C. Dri, M. Panighel, D. Tiemann, L. L. Patera, G. Troiano, Y. Fukamori, F. Knoller, B. A. J. Lechner, G. Cautero, D. Giuressi, G. Comelli, J. Fraxedas, C. Africh, and F. Esch, "The new FAST module: A portable and transparent add-on module for time-resolved investigations with commercial scanning probe microscopes," Ultramicroscopy **205**, 49–56 (2019).

[14]C. Xu, Y. Que, Y. Zhuang, K. Wang, and X. Xiao, "Construction of a gigahertz-bandwidth radio-frequency scanning tunneling microscope based on a commercial low-temperature system," Rev. Sci. Instrum. **90**, 103706 (2019).

[15]Q. F. Li, Y. Wang, F. Wang, Y. Hou, and Q. Lu, "100 MHz large bandwidth preamplifier and record-breaking 50 kHz scanning rate quantum point contact mode probe microscopy imaging with atomic resolution," Rev. Sci. Instrum. **92**, 013701 (2021).

[16]C. Dri, F. Esch, C. Africh, and G. Comelli, "How to select fast scanning frequencies for high-resolution fast STM measurements with a conventional microscope," Meas. Sci. Technol. **23**, 055402 (2012).

[17]Y. I. Yanson, F. Schenkel, and M. J. Rost, "Design of a high-speed electrochemical scanning tunneling microscope," Rev. Sci. Instrum. **84**, 023702 (2013).

[18]H. Yamashita, N. Handa, Y. Higashiura, and M. Abe, "Flexure structural scanner of tip scan type for high-speed scanning tunneling microscopy," e-J. Surf. Sci. Nanotechnol. **18**, 146–151 (2020).

[19]J. Wintterlin, J. Trost, S. Renisch, R. Schuster, T. Zambelli, and G. Ertl, "Real-time STM observations of atomic equilibrium fluctuations in an adsorbate system: O/Ru(0001)," Surf. Sci. **394**, 159–169 (1997).

[20]S.-K. Hung, "Spiral scanning method for atomic force microscopy," J. Nanosci. Nanotechnol. **10**, 4511–4516 (2010).

[21]Y. K. Yong, S. O. R. Moheimani, and I. R. Petersen, "High-speed cycloid-scan atomic force microscopy," Nanotechnology **21**, 365503 (2010).

[22]I. A. Mahmood, S. R. Moheimani, and B. Bhikkaji, "A new scanning method for fast atomic force microscopy," IEEE Trans. Nanotechnol. **10**, 203–216 (2011).

[23]A. Bazaei, Y. K. Yong, and S. O. R. Moheimani, "High-speed Lissajous-scan atomic force microscopy: Scan pattern planning and control design issues," Rev. Sci. Instrum. **83**, 063701 (2012).

[24]Y. K. Yong, A. Bazaei, S. O. R. Moheimani, and F. Allgöwer, "Design and control of a novel non-raster scan pattern for fast scanning probe microscopy," in *IEEE/ASME International Conference on Advanced Intelligent Mechatronics (AIM)* (IEEE, 2012), pp. 456–461.

[25]Y. K. Yong, A. Bazaei, and S. R. Moheimani, "Video-rate Lissajous-scan atomic force microscopy," IEEE Trans. Nanotechnol. **13**, 85–93 (2014).

[26]X. Sang, A. R. Lupini, R. R. Unocic, M. Chi, A. Y. Borisevich, S. V. Kalinin, E. Endeve, R. K. Archibald, and S. Jesse, "Dynamic scan control in STEM: Spiral scans," Adv. Struct. Chem. Imaging **2**, 6 (2016).

[27]Z. Sun, N. Xi, Y. Xue, Y. Cheng, L. Chen, R. Yang, and B. Song, "Task space motion control for AFM-based nanorobot using optimal and ultralimit Archimedean spiral local scan," IEEE Rob. Autom. Lett. **5**, 282–289 (2020).

[28]J. Wang, G. Zhang, and Z. You, "Design rules for dense and rapid Lissajous scanning," Microsyst. Nanoeng. **6**, 101 (2020).

[29]S. B. Andersson and D. Y. Abramovitch, "A survey of non-raster scan methods with application to atomic force microscopy," in *2007 American Control Conference* (IEEE, 2007), pp. 3516–3521.

[30]J. Wang, J. Wang, Y. Hou, and Q. Lu, "Self-manifestation and universal correction of image distortion in scanning tunneling microscopy with spiral scan," Rev. Sci. Instrum. **81**, 073705 (2010).

[31]D. Ziegler, T. R. Meyer, R. Farnham, C. Brune, A. L. Bertozzi, and P. D. Ashby, "Improved accuracy and speed in scanning probe microscopy by image reconstruction from non-gridded position sensor data," Nanotechnology **24**, 335703 (2013).

[32]M. S. Rana, H. R. Pota, and I. R. Petersen, "Spiral scanning with improved control for faster imaging of AFM," IEEE Trans. Nanotechnol. **13**, 541–550 (2014).

[33]D. Ziegler, T. R. Meyer, A. Amrein, A. L. Bertozzi, and P. D. Ashby, "Ideal scan path for high-speed atomic force microscopy," IEEE/ASME Trans. Mechatron. **22**, 381–391 (2017).

[34]S. K. Das, F. R. Badal, M. A. Rahman, M. A. Islam, S. K. Sarker, and N. Paul, "Improvement of alternative non-raster scanning methods for high speed atomic force microscopy: A review," IEEE Access **7**, 115603–115624 (2019).

[35]H. Over, "Surface chemistry of ruthenium dioxide in heterogeneous catalysis and electrocatalysis: From fundamental to applied research," Chem. Rev. **112**, 3356–3426 (2012).

[36]S. H. Pan, E. W. Hudson, and J. C. Davis, "^{3}He refrigerator based very low temperature scanning tunneling microscope," Rev. Sci. Instrum. **70**, 1459–1463 (1999).

[37]W. E. Norum, "EPICS on the RTEMS real-time executive for multiprocessor systems," Rev. Sci. Instrum. **73**, 1560–1562 (2002).

[38]S. Veseli, "PvaPy: Python API for EPICS PV access," in Proceedings of ICALEPCS (2015).

[39]K. Shroff, C. Rosati, G. Weiss, K. Kasemir, and E. Smith, "New Java frameworks for building next generation EPICS applications," in *17th International Conference on Accelerator and Large Experimental Control Systems (ICALEPCS2019)* (2019), http://www.jacow.org.

[40]H. Junkes, H.-J. Freund, L. Gura, M. Heyde, P. Marschalik, and Z. Yang, "Experiment control with EPICS7 and symmetric multiprocessing on RTEMS," in *16th International Conference on Accelerator and Large Experimental Control Systems (ICALEPCS2017)* (2018), http://www.jacow.org, pp. 1762–1766.

[41]G. Schitter, "Advanced mechanical design and control methods for atomic force microscopy in real-time," in *2007 American Control Conference* (IEEE, 2007), pp. 3503–3508.
[42]S. Yang and W. Huang, "Transient responses of a piezoelectric tube scanner," Rev. Sci. Instrum. **68**, 4483–4487 (1997).
[43]S. Yang and W. Huang, "Three-dimensional displacements of a piezoelectric tube scanner," Rev. Sci. Instrum. **69**, 226–229 (1998).
[44]M. E. Taylor, "Dynamics of piezoelectric tube scanners for scanning probe microscopy," Rev. Sci. Instrum. **64**, 154–158 (1993).
[45]M. B. Leonard Gura, see https://github.molgen.mpg.de/gura/point_cloud_visualization_and_analyis for "Point Cloud Visualization and Analysis, GitHub repository, 2021."
[46]S. van der Walt, J. L. Schönberger, J. Nunez-Iglesias, F. Boulogne, J. D. Warner, N. Yager, E. Gouillart, T. Yu, S. Gomez, and scikit-image contributors, "scikit-image: Image processing in Python," PeerJ **2**, e453 (2014).
[47]P. Virtanen, R. Gommers, T. E. Oliphant, M. Haberland, T. Reddy, D. Cournapeau, E. Burovski, P. Peterson, W. Weckesser, J. Bright, S. J. van der Walt, M. Brett, J. Wilson, K. J. Millman, N. Mayorov, A. R. J. Nelson, E. Jones, R. Kern, E. Larson, C. J. Carey, İ. Polat, Y. Feng, E. W. Moore, J. VanderPlas, D. Laxalde, J. Perktold, R. Cimrman, I. Henriksen, E. A. Quintero, C. R. Harris, A. M. Archibald, A. H. Ribeiro, F. Pedregosa, P. van Mulbregt, and SciPy 1.0 Contributors, "SciPy 1.0: Fundamental algorithms for scientific computing in Python," Nat. Methods **17**, 261–272 (2020).